Proceedings of ASME Turbo Expo 2011
GT2011
June 6-10, 2011, Vancouver, British Columbia, Canada

GT2011-45094

THE EFFECTS OF RADIALLY DISTORTED INCIDENT FLOW ON THE PERFORMANCE OF AXIAL-FLOW FANS WITH FORWARD-SKEWED BLADES

B. Yang
School of Mechanical Engineering,
Shanghai Jiaotong University
Shanghai, China

Ch. G. Gu
School of Mechanical Engineering,
Shanghai Jiaotong University
Shanghai, China

ABSTRACT

In this study, the experiments and simulations have been carried out to evaluate the effects of radially distorted incident flow on the performance of axial-flow fans equipped with forward-skewed blades. These fans were manufactured with different forward-skewed angle, such as 3°, 6° and 12° respectively. Based on the experimental and numerical results, it is found that under the uniform inlet condition the fan with the 12° forward-skewed angle manifests the most excellent performance, and its peak efficiency is increased by 6.27% and 3.41% respectively in comparison with those of two other fans. However, when a hub-covered screen is mounted and then the uniform inlet condition is consequently destroyed, the peak efficiency of all three fans is decreased by more than 2.8%. Under the third inlet condition, as the main stream is compelled towards blade hub by a tip-covered screen, the effect of forward-skewed blades on the fan performance is reinforced and fan performance is improved. In order to get further understanding, contours of the loss coefficient and the axial velocity at exit have also been studied both at the design point and the lower mass rate point. All results exhibit that there are beneficial effects of forward-skewed blades on fan performance and the performance is quite sensitive to radially distorted incident flow. Furthermore, rotating stall has been observed by use of three dynamic pressure sensors. The instantaneous results reveal that when the fans are operated with different kinds of incident flow, pressure fluctuations with time have different modes as the fans are sliding down into rotating stall.

INTRODUCTION

Axial-flow compressor, turbine and fan are now playing an important role in civilian and military applications. High performance and lower noise are always important issues in the designs of these kinds of axial-flow turbomachinery. In the present stage of their development, an assumption, i.e. uniform inlet condition, has been widely accepted and used in most of practical cases. However, the assumption has seldom been matched by real working conditions because of machine-inlet configurations or inlet boundary interaction or atmospheric turbulence. Additionally, the instability, such as rotating stall and surge which can give rise to unsteady blade force and vibration and then lead to catastrophic damage to the entire machine, can be easily activated and aggravated by poor inlet condition. Consequently, for an advanced design, it is necessary to seek to get some valuable knowledge of the effects of distorted or non-uniform incident flow on performance of the turbomachinery.

Non-uniform incident flow can manifest themselves in either temperature field, pressure field, or both. But, until now the most common type of distorted inlet condition in axial-flow turbomachinery is distorted inlet total pressure. Related to D.P. Harry [1], he investigated a turbojet engine to determine the effects of uneven inlet pressure distributions, such as circumferential, radial and mixed distortion, on transient characteristics and on rotating stall. In one of earlier researches, D.M.Sandercock [2] did experiments with radially distorted incident flow. He found that there was a general decrease in pressure ratio and a decrease in the rotor stall margin with top radial distortion, while with hub radial distortion there was no change or some increase in pressure ratio and rotor stall margin.

In recent years, the great efforts have been made in some experimental researches in which performance of axial-flow compressor related to some special distortion in inlet total pressure has been studied. Z.S. Spakovszky [3] represented a kind of active rotating stall control in a transonic compressor and studied the stall inception pattern with radial inlet distortion. D.C. Leinhos [4] tested the influence of transient inlet distortion on the inception of instability in a low-pressure compressor. Meanwhile, some numerical simulations on the machine performance with several kinds of distortion in incident flow have been reported. R. V. Chima [5] presented unsteady flow simulation with radial and circumferential distortion by means of 3D code. C. Hah [6] provided the effects of circumferential distortions in inlet total pressure on the pattern of the flow field in a low-aspect-ratio, high-speed, high-pressure-ratio, transonic compressor rotor. Also, the problem of inlet distortion has always been one of the major concerns in the field of axial-flow fan design and maintenance. Salta [7] did experiments to study the effects of distortion in incident flow on the performance of an axial-flow fan used in air-cooled exchangers. Ch. Jang [8] investigated distorted incident flow induced by various types of hub caps, and analyzed its effects on performance of a kind of axial-flow fan.

In a further aspect, in order to maintain the safe and efficient operation, forward-skewed blades have been introduced in the design of axial-flow turbomechinery. In the early of 1960s, a relationship between cascade solidity and attack angle was presented in detail by Smith [9]. The research to utilize skewed blades in the design of a low-speed machine was done by S.J.Gallimore [10]. It was found that the forward-skewed blades could effectively reduce the hub corner and tip clearance loss by comparing the overall performance of the impellers, which were equipped with forward-skewed, radial and backward-skewed blades respectively. Beiler and Carolus [11, 12] pointed out that the forward-skewed blades could lead to more uniform distribution of aerodynamic parameters at outlet and then reduce the dynamic discharge losses. The improved acoustic performance could also be expected. Breugelmans and Sasaki [13, 14] demonstrated that the profits from the forward-skewed blades might be due to the control of local pressure gradient within the flow passage.

However, though the importance of the effects of distorted incident flow on performance of axial-flow turbomechinery has already been recognized and the feasibility of design method adopting forward-skewed blades to improve machine performance has already been validated, very few research have been reported to investigate the effects of distorted incident flow on performance of axial-flow turbomechinery with forward-skewed blades and the assumption of uniform inlet condition has been still widely accepted in the designs of blades with skewed profiles. Indeed, to some degree, the assumption has hampered the development of the modern design methodology of turbomechinery and weakened the expected benefit from forward-skewed blades.

The present paper describes a study in which the efforts are made to illustrate the effects of radially distorted incident flow on pattern of the flow field of a kind of axial-flow fan with forward-skewed blades. Under the different distorted inlet conditions, performance of three axial-flow fans with different forward-skewed angles has been investigated by means of experiments and numerical simulations. Discussion of the effects of distorted incident flow on rotating stall and on some critical aerodynamics parameters is also included. But, it is necessary to state that the described study is based on low speed axial-flow machine. For high speed compressor or fans, especially when blade tip flow is transonic, the effects of forward swept or skewed blades upon performance can be very different from those obtained from low speed machines.

NOMENCLATURE

C_p	total pressure coefficient
Q	fluid rate
S	area of measurement section
p	pressure
r	radius
v	absolute velocity
w	relative velocity
ϕ	flow coefficient
λ	relative blade length
θ	skewed forwards angle
ρ	density
ω_x	loss coefficient
superscript	
$*$	total parameter
Subscript	
0	atmospheric parameters
1	inlet section
2	outlet section
h	blade hub
t	blade tip

EXPERIMENT SETUP

The Forward-Skewed Blade

In this paper, the forward-skewed angle is defined as shown in Fig. 1. According to the drawing, a circular arc is adopted as the stacking line, and O' is the center of the arc. H is the intersection point between hub line and stacking line, T is the intersection point between shroud line and stacking line, C is a random point on the stacking line. The line OH is assumed to be perpendicular to $O'H$. Then, θ is defined as forward-skewed angle and can be obtained by the following equation.

$$\theta(r) = \theta_{o'} - \arccos\left(\frac{(r^2 + r_{o'}^2 - R_M^2)}{2rr_{o'}}\right) \tag{1}$$

where, r is the radius of the point C, R_M is radius of the stacking line which can be calculated by the Eq. (2).

$$R_M = \frac{r_t}{2\sin\theta_t}(\sin^2\theta_t + (\cos\theta_t - \frac{r_h}{r_t})^2) \tag{2}$$

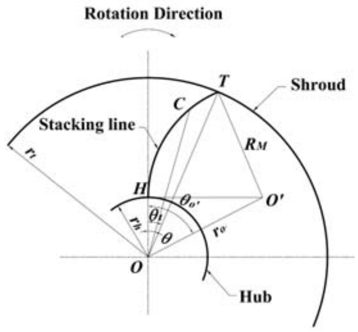

Fig. 1 scheme of definition of forward-skewed angle

where, r_h and r_t are radius of the hub and the shroud respectively, θ_t is skewed forward angle at the blade tip. $r_{o'}$ and $\theta_{o'}$ can be determined respectively by following equations.

$$r_{o'} = \sqrt{r_h^2 + R_M^2} \tag{3}$$

$$\theta_{o'} = \arctan(R_M / r_h) \tag{4}$$

Therefore, once is θ_t settled, other forward-skewed angles of all sections along entire span should be determined consequently.

Test Fans

Table 1 key parameters of the axial-flow fan

Parameters	*Symbol*	*Unit*	
	Aerodynamic		
Volume Rate	Q	m^3/h	31000
Inlet Temp.	T_1	^{o}C	20
Inlet Total Pres.	p_0	Pa	101300
Static Pre. Increase	Δp_{st}	Pa	210
	Geometric		
Diameter of Impeller	D_2	mm	900
Tip/Hub Ratio			3
Blade Solidity			0.698

A kind of axial-flow fan, which is low speed axial machine and designed for an evaporator, has been adopted in this research. The key parameters are shown in Table 1. Its origin θ_t is only three degree. In order to carry out the comparative experiments and numerical simulations and to illustrate the performance difference among fans with different skewed blades, two other fans with different θ_t, i.e. 6° and 12°, have been observed as well, as shown in Fig. 2.

The Spherical Seven-hole Probes

In order to get detail information on flow field of the fans, two specific seven-hole probes have been designed and mounted at inlet and outlet of the impellers respectively. The spherical seven-hole probe is different from a conical seven-hole probe. The arrangement of seven holes is shown in Fig. 3.

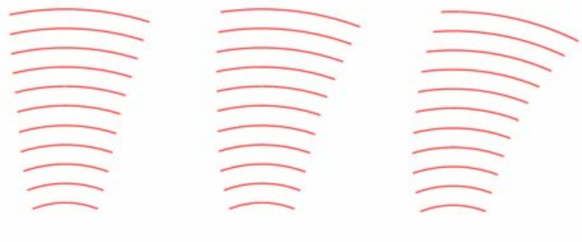

(a) 3^o (b) 6^o (c) 12^o

Fig. 2 three blades with different forward-skewed angles

Fig. 3 seven-hole probe

The measurement range is therefore extended to within ± 85º in the pitch plane. And its calibration process is much simpler than that of a conical seven-hole probe. In fact, it is reasonable to consider that a spherical seven-hole probe consists of three separated five-hole probes, e.g. 1-2-3-4-5, 1-2-3-5-6, and 1-2-3-6-7. As the pitch angle of a velocity is within the range of from 25 to 85 degree, the measurement is related to the holes group 1-2-3-4-5; as within the range of ± 30 degree, to the holes group 1-2-3-5-6; as within the range of from -85 to -25 degree, to the holes group 1-2-3-6-7. So, the calibration of this seven-hole probe can be simplified to calibrate three five-hole probes at 5 degree intervals both in yaw and in pitch planes. The calibration curves and calibration process of this kind of seven-hole probe are quite similar to those of a five-hole probe. During the process of calibration, it is unnecessary to divide the calibration region into seven zones, such as one central zone and six side zones, which are usually described in user manual of a kind of conical seven-hole probe.

Nevertheless, the observation range of pitch angle from the spherical seven-hole probe is not wide enough to get full information about velocity due to negative velocity component (opposite to inflow direction) at fan exit. So, during the experiment, when the pitch angle exceeds certain degree, it needs to turn the probe 180º.

Experimental Facility

The whole test rig, showed in Fig. 4, has been set up in accordance with Standard GB/T 2888-91 [15].

Since the researches have been focused on radially distorted incident flow, three screens, such as an even screen, a tip-covered screen and a hub-covered screen, are adopted to produce three kinds of incident flow by being mounted on a carrier. Moreover, DANTEC Streamline System is used to measure turbulence intensity ($U'/U(R)$) for determining suitable screen-to-impeller relative distance in order to elimina-

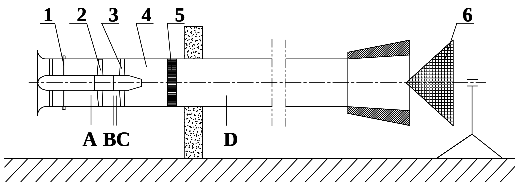

1. Screen Carrier 2. Impeller 3. Motor 4. Test Tube 5. Straightening Screen 6 Conical Throttle
A. 7-Hole Probe at inlet of impeller B. 7-Hole Probe at outlet of the impeller C. Dynamic Pressure Sensors D. Pitot Probe
Fig. 4 scheme of experimental rig

te unsteady effects due to flow separation in the downstream of a screen. When the distance between probe and screen is adopted as much as 1.5 blade height, it is found that the turbulent intensity is about 2.7% near the tube wall, but it is less than 0.88% in the mainstream. So, it is believed that when the screen-to-impeller relative distance is adopted over certain degree, i.e. 1.5 blade height upstream from an impeller, the distortions in incident flow are purely radial and have nothing to do with unsteady effects.

Three Kulite dynamic pressure sensors, model XTL-190M, are mounted at exit to capture the pressure fluctuation in the downstream of a impeller, which are fixed at different radial position, such as 15%, 50% and 85% of blade height. Volume rate can be adjusted by pulling or pushing the conical throttle on a rail in axial direction at outlet of the wind tube. A pitot probe is used to measure volume rate. Since axial velocity in the wind tube is often fluctuated along entire span, especially under certain kind of radially distorted inlet condition, it is necessary to measure axial velocity at different points along entire span on the test section and then integrate to get more accurate mass flow rate. And in order to suppress the measurement error as far as possible, two digital micromanometers are connected with the pitot probe.

Three dynamic pressure sensors and two digital micro-manometers for pitot probe as well as several static pressure transducers for transferring pressure signals from seven-hole probes are all connected to PC through a data acquisition system based on Labview. The detail configuration of the measurement instruments is shown in Fig. 5.

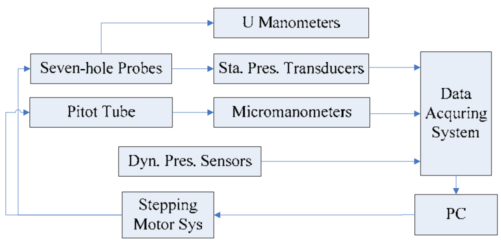

Fig. 5 instruments arrangement

Accuracy

In respect of the seven-hole probe, considering some effects on the measurement accuracy, such as Reynolds number, velocity gradient, turbulence level in incident flow and interpolating by use of calibration curves, the errors in flow angles are found to be within $\pm 1°$ and the errors in total and static pressures are within 0.4% and 0.9% of the dynamic pressure respectively. Accuracy of the measurement of the transient pressure is maintained at such level that three sensors are accurate to $\pm$0.0015atm. The accuracy of pitot probe for volume rate measurement is $\pm$0.0035atm. In order to reduce the effect of noise or scatter on the measurements, all of measurements of static parameters are averaged.

NUMERICAL SIMULATION

3D numerical simulations of RANS equations are adopted to evaluate the performance of the axial-flow fans. In some cases, k-ω model has exhibited excellent ability to simulate flow with fiercely adverse pressure gradient[16, 17, 18]. Furthermore, in this model, the parameters, such as k and ω, can be integrated directly through viscous sublayer without the aid of viscous damping functions. Wilcox [16] had compared the simulation results and found that skin friction predicted by k-ω was perfectly approved by the measured results. Yang [18] also had proved that k-ω model was suitable to simulate flow around airfoil with high attack angle. In this research, in order to study fan performance with lower mass flow, sometimes the working points are set much close to rotating stall point. Then, a large amount of adverse flow and vortex are bound to be found at these working points. Therefore, the k-ω turbulence model should be suitable to be selected to close RANS equations.

A commercial CFD code, Fine/Turbo™[19], is used to compute the flow field. The value of CFL is adopted as 3. Reynold number is about 6×10^5 when the blade chord is adopted as characteristic length.

The computational mesh is of $85\times73\times361$ nodes respectively in pitch, span and stream wise directions. Multi-grid strategy is also introduced in this research and the mesh used to simulate the space has multiple grid levels in three directions. The value of y^+ near the solid wall is guaranteed less than 2. No slip and no heat transfer conditions are imposed on solid boundaries. As far as the inlet boundary conditions are concerned, specified profiles are adopted. During experiments, when an uneven screen is mounted, the profile of velocity as well as that of total pressure is greatly affected along radial direction. In fact, there is still a little distortion of velocity and total pressure when the uniform screen is equipped, especially in the region near the tube wall. So, the profiles of velocity, total pressure and total temperature are all provided strictly in accordance with experimental conditions measured at position A, as shown in Fig.4. The section A is extended 100% of chord length upstream of an impeller. The static pressure is imposed at outlet and the outlet section is extended 150% of chord length downstream.

RESULT AND ANALYSIS

Some key dimensionless parameters are defined as following, such as flow coefficient, total pressure coefficient, relative blade length and loss coefficient.

$$\phi = \frac{Q}{S \times \sqrt{p_0 / \rho}} \cdot 10^3 \tag{5}$$

$$C_p = \frac{p_2^* - p_1^*}{p_0} \cdot 10^3 \tag{6}$$

$$\lambda = \frac{r - r_h}{r_t - r_h} \tag{7}$$

$$\omega_x = \frac{p_{w1}^* - p_{w2}^*}{\frac{\rho w_1^2}{2}} \tag{8}$$

where Q is volume rate, S area of measurement section, ρ air density, p_0 atmospheric pressure, p_1^* and p_2^* total pressure at the inlet and the outlet respectively, w_1 relative velocity at the inlet, p_{w1}^* and p_{w2}^* relative total pressure at the inlet and the outlet respectively.

Fan Performance

These fans are tested with three different radially distorted incident flow, i.e. one uniform and two radially distorted. At impeller exit, the loss coefficient and velocity components are observed at two points, i.e. $\varphi = 46.6$ and $\varphi = 45.1$. The former is the design point and the later is one of off-design points with the lower mass flow rate. In addition, another characteristic point, the lowest mass flow point, is also investigated, which is quite close to rotating stall. The mass flow rate at the point can present rotor stall margin and illustrate range of stable operation of machine. In this study, it is determined by the following steps. When the conical throttle (labeled 6 in Fig. 4) is pushed to a certain position and fierce fluctuations of static pressure from dynamic pressure sensors can be clearly observed on the monitor, it demonstrates that the fan is about to slide down into the rotating stall condition. So, it is necessary to gradually pull the conical throttle back somewhat till the pressure fluctuations totally disappear from the monitor. The position of the conical throttle is recorded and the rate of mass flow is measured subsequently. In order to reduce the effect of measurement noise, this process has to be reiterated for several times, and then the point is regarded as the lowest mass flow point.

Through comparing results, agreement between experimental data and simulation data is so good that the valuable appreciation about fan's characteristic can be expected on the basis of these results.

Uniform Inlet Condition

Overall performance

When the uniform screen is mounted on the carrier, it is observed that the distribution of aerodynamic parameters, such as velocity and pressure, are almost uniform along radial direction except the relatively small domain close to the tube walls.

It is shown in Fig.6 that the fan with 12° forward-skewed angle manifests the most excellent performance. In Fig. 6(a), its peak efficiency is increased by 6.27% and 3.41% respectively in comparison with those of two other fans with 3° and 6° forward-skewed angle. It also indicates that difference of overall performance among three fans is not high at high mass flow whereas at low mass flow, the difference is more. Similar results have been reported by Yamaguchi[20] and Govardhan[21]. Furthermore, through comparing the lowest mass flow points of these three fans, it is found that the stable operating range is really improved to some extend with increasing of the forward-skewed angle. The lowest mass flow rate developed by the fan with 12° forward-skewed angle is lower than that of the fan with 3° forward-skewed angle by about 2.57%. But, as the forward-skewed angle is increased, the pressure rise from the impeller is reduced, as shown in Fig 6(b). Additionally, the difference in pressure rise between 3° forward-skewed fan and 6° forward-skewed fan seems not to be very distinct, while the difference between 3° forward-skewed fan and 12° forward-skewed is relatively obvious.

With respect to the radial blades adopted in the axial-flow turbomachinery, the mainstream as well as inertial flow in boundary layer is generally compelled towards blade tip by centrifugal force, and inertial flow is especially apt to be accumulated in the area around suction side at the tip. As a result, the risks of flow separation and leakage become higher, and the machine is likely to slide down into the rotating stall condition. In order to alleviate this situation, the forward-skewed blade has been introduced in the fan design and is believed to have a kind of ability to improve fan performance, which has already been proved by many published researches. In general, it is considered the forward-skewed blades can introduce a kind of radial force, direction of which is opposite to that of

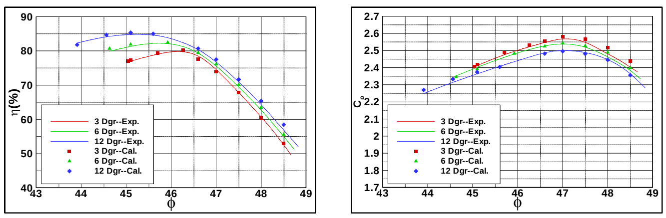

(a) efficiency **(b) total pressure coefficient**

Fig. 6 fan performance under uniform inlet condition

centrifugal force. Therefore, the mass movement from hub to tip is effectively controlled, more part of fluid is compelled to flow through lower part of flow passage and then the thickness of boundary layer around the blade tip area is actually thinned. And, it is more important that at this moment the blade loading around tip area is effectively reduced and uniformity of loading along entire span is promoted. So, it can be concluded that the forward-skewed blades can reduce the mass flow around tip area, release excessive blade loading in this area and consequently enhance the whole performance of the machine. But, because wheel speed near the hub is lower than that of the tip, transferring mass from upper part of the flow passage to lower part must lead to decreasing of total work on the fluid, as shown in Fig. 6(b).

Design Point

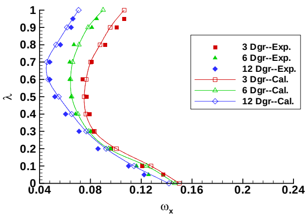

Fig. 7 distribution of loss coefficient along spanwise at design point under uniform inlet condition

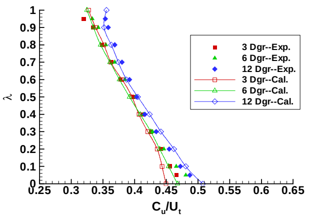

Fig. 8 distribution of tangential velocity coefficient along spanwise at design point under uniform inlet condition

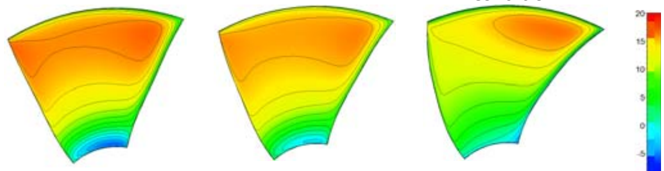

(a) 3° **(b) 6°** **(c) 12 °**

Fig. 9 contours of axial velocity at design point under uniform inlet condition

Fig. 7 shows the comparison of pressure loss coefficient among three fans at the design point, obtained from experiments and numerical simulations. In the case of the fan with 3° forward-skewed angle, the small loss coefficient is found in blade tip and the mid-span region, while in the hub region the loss coefficient is increased drastically. Meanwhile, the fans with angle 6° and 12° have similar curve tendencies, but their values are lower than the former, especially in the tip region. At 90% of span of the blade from the hub, the loss coefficient developed by 12° forward-skewed blade is lower than that of 3° forward-skewed fan by about 55.25%, 48.08%at span 50%, and 9.63% at span 10%. The loss that occurs near hub is mainly due to corner vortex in this region, which will be discussed in later section. Though the vortex can be pressed by forward-skewed blades to a certain small size, it is still presented more or less near the hub. As a result, the relatively high aerodynamic loss near blade hub is inevitable.

The comparison of distribution of tangential velocity at exit is described in Fig. 8. It reveals that the tangential velocity of 12° forward-skewed fan is higher than two other fans along entire span. Other results about velocity component from CFD are shown in Fig. 9. They are the figures of axial velocity contours at exit. As shown in Fig.9, the negative velocity can be obviously found in the area near the blade hub, which can give rise to certain amount of aerodynamic loss. And from Fig. 9(a) to Fig. 9(b) and then Fig. 9(c), it may also be found that with increasing of forward-skewed angle, the size of region of the negative velocity is gradually diminished, distribution of the axial velocity delightfully becomes more uniform and aerodynamic loss is consequently reduced. From these results about velocity component distribution as well as loss coefficient, it can confirm conclusion obtained from analysis of overall performance. Forward-skewed blade can literally adjust distribution of mass flow along entire span and improve its uniformity so that the loading near blade top is released somewhat and fan performance is achieved.

Lower mass flow point

Distribution of loss coefficient of three fans with the lower mass flow rate is presented in the Fig 10. It is found that the coefficient of all three fans is obviously increased in comparison with those at design point. Especially, at mid-span, the changing is drastically. At 50% span, the coefficient of fan with 3° forward-skewed angle is increased by 36.68% in comparison with results obtained at design point, while the coefficient of the fans with 6° forward-skewed angle and with 12° forward-skewed angle is increased by 42.8% and 34% respectively. Theoretically, it is no doubt that the fan performance usually is not very desirable at the points with lower mass flow because these points actually drift far away from fan's design point.

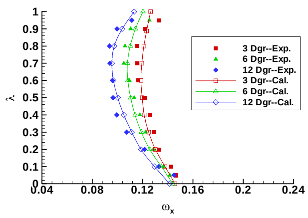

Fig. 10 distribution of loss coefficient along spanwise at lower mass flow point under uniform inlet condition

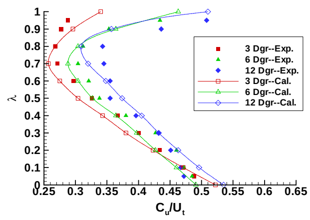

Fig. 11 distribution of tangential velocity coefficient along spanwise at lower mass flow point under uniform inlet condition

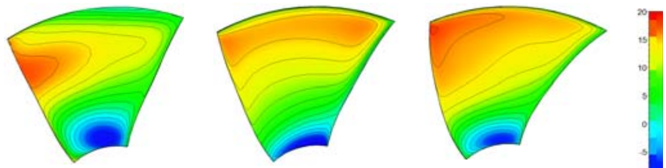

(a) 3° **(b) 6°** **(c) 12 °**

Fig. 12 contours of axial velocity at lower mass flow point under uniform inlet condition

Under this condition, incidence angle usually exceeds reasonable level so that it can lead to serious separation at blade leading edge close to suction side of blade, and then give rise to consequent aerodynamic loss.

In order to get further understanding, distributions of tangential velocity and contours of axial velocity are shown in Fig. 11 and Fig. 12 respectively. It is found in Fig.11 the difference among three curves becomes more distinct, especially near to blade tip region. At 90% span, the tangential velocity of the fan with 3° forward-skewed angle is lower 47.8% than that of 12° forward-skewed fan. Therefore, it can conclude that the effect of forward-skewed blades on fan performance is more at low mass flow. In Fig.12, the hub region is now preoccupied by the negative axial velocity and flow separation is thereby relatively serious in this region. This larger back-flow region is considered to be big enough to affect the flow around blade mid-span, and as a result the flow around mid-span is sharply deteriorated and the excessive aerodynamic loss can be observed in this region, which is in accordance with the phenomena described in Fig.10.

Hub-covered Distorted Inlet Condition

Overall performance

The hub-covered screen, which consists of a fine mesh covering 30% of blade height in the hub region, is mounted on the carrier to produce a kind of radially distorted incident flow.

It is found that under this condition, even if the machines are operated at design point which is very close to peak efficiency point, the performance is not preferable. The peak efficiency of three fans is decreased by more than 2.8% as shown in Fig.13(a) in comparison with that obtained under uniform inlet condition. And, the lowest mass flow of three fans is moved to bigger mass flow point and the rotating stall margin is consequently shortened. It is also found performance curves of three fans seem to become more close to each other, i.e. the peak efficiency of the fan with 12° forward-skewed angle is only higher than that of the fan with 3° forward-skewed angle by about 3.81%. Similar phenomenon is also observed in Fig. 13 (b).

In this case, when the hub-covered screen is mounted, an amount of fluid is bound to be pressed into upper part of flow passage. Then, it is believed that the effect of forward-skewed on the fan performance is weakened and performance difference among three fans is narrowed. In other words, though there are still some positive effects of forward-skewed blades on the fan performance, no longer can boundary layer accumulation close to tip region be effectively controlled. As a result, the flow situation in the tip region and even in the mid-span region has not been improved to an expected degree, and consequently overall performance is implicated. So, if a fan with forward-skewed blade is designed based on the assumption of uniform inlet condition, which is general accepted in most industrial application, it is believed that benefit from forward-skewed blade can not be completely realized when the fan is operated under practical condition in one form or another which is like the condition produced by the hub-covered screen. It suggests that under this kind of condition the need of a higher forward-skewed angle for realizing expected benefit is essential.

Design Point

Distribution of loss coefficient at the design point is depicted in Fig. 14. It is found that at the moment the loss coefficient from hub to tip is higher than that obtained under uniform inlet condition with the corresponding mass flow rate. The coefficient is particularly increased around mid-span area. At 50% span, the coefficient of the fan with 12° forward-skewed angle is increased by about 35.77%, as those of the fans with 6° forward-skewed angle and 3° forward-skewed angle are increased by about 27.16% and 14.29% respectively.

The comparison of distribution of the tangential velocity at exit is made in Fig. 15. Though it still indicates that the tangential velocity of the fan with 12° forward-skewed angle is higher than two other fans along entire span, the difference is not as big as that obtained under uniform condition. On the other hand, the larger corner vortex near blade hub can be found in Fig. 16. It is

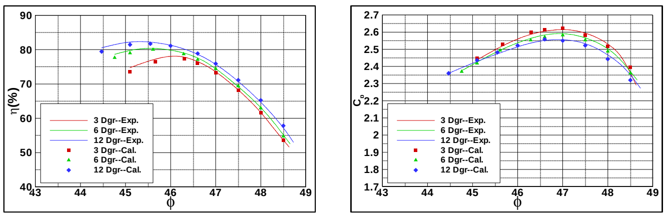

(a) efficiency **(b) total pressure coefficient**

Fig. 13 fan performance under hub-covered inlet condition

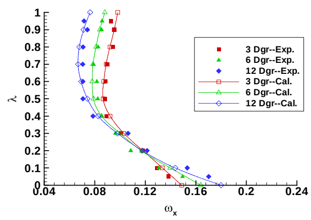

Fig. 14 distribution of loss coefficient along spanwise at design point under hub-covered inlet condition

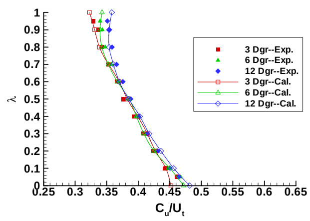

Fig. 15 distribution of tangential velocity coefficient along spanwise at design point under hub-covered inlet condition

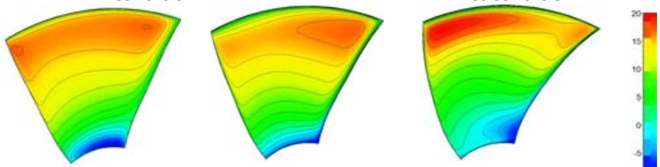

(a) 3° **(b) 6°** **(c) 12 °**

Fig. 16 contours of axial velocity at design point under hub-covered inlet condition

observed that negative velocity is spread to more extensive region, despite the size of the corner vortex become smaller with increasing of forward-skewed angle.

Lower mass flow point

Under this condition, the comparison of distribution of loss coefficient along entire span is shown in Fig. 17. Granted, the difference between simulations and experiments seems to be not ideal, the maximum value of which is about 16.7% at hub. It is so much because the 7-hole probe suffers from this working condition. Under the condition, the back-flow region near blade hub becomes so big and trailing edge of the blade is therefore so strong that it must bring excessive measurement errors and hardly precisely determine the velocity vector. By the way, it is extremely difficult to diminish completely errors from turbulence model, discreteness scheme and grid strategy which are adopted in the paper. Nevertheless, it still illustrates the flow situation becomes more deteriorated. From 50% span to hub, the loss coefficient of all three fans is drastically increased. The maximum coefficient near the hub of the fan with 3° forward-skewed angle is about 0.229 (from numerical simulation).

Distributions of tangential velocity and the contours of axial velocity are shown in Fig. 18 and Fig. 19 respectively. It is shown in Fig. 18 that the curves of tangential velocity distribution under this condition present a trend which is similar to that obtained under even inlet condition (shown in Fig. 11). But, the contours of axial velocity are rather different. In these cases, as shown in Fig. 19(a), (b) and (c), the scale of negative velocity is further enlarged and almost a third of blade height from hub is occupied by the vortex. More proportion of mass flow is compelled toward the blade tip so that the distribution of axial velocity becomes more non-uniform and the loading in the tip region becomes very heavy. The flow becomes totally unfavorable, especially in the hub region where the flow separation is so

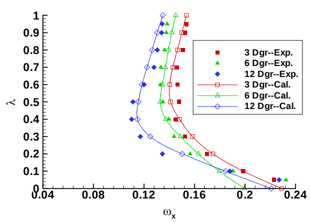

Fig. 17 distribution of loss coefficient along spanwise at lower mass flow point under hub-covered inlet condition

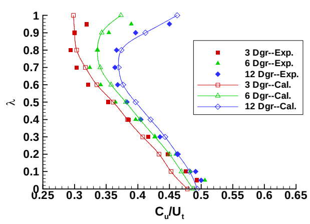

Fig. 18 distribution of tangential velocity coefficient along spanwise at lower mass flow point under hub-covered inlet condition

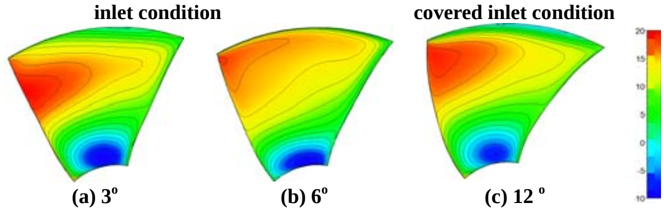

(a) 3° **(b) 6°** **(c) 12 °**

Fig. 19 contours of axial velocity at lower mass flow point under hub-covered inlet condition

serious that the stall cells will be found in flow passage sooner or later. This set of data about velocity components also can be used to explain why the loss coefficient of all three fans is drastically increased (shown in Fig. 17).

It is observed from Fig.13 that the lower mass flow point is much more close to the lowest mass flow (In fact, in the case of the fan with 3° forward-skewed angle, the working point of $\varphi = 45.1$ is already degraded to the lowest mass flow point). It means that three fans are much more likely to slide down into rotating stall even at relative higher mass flow, especially for the fan with 3° forward-skewed angle.

Tip-covered Distorted Inlet Condition

Overall performance

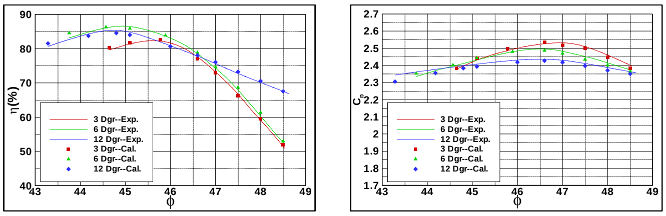

(a) efficiency **(b) total pressure coefficient**

Fig. 20 fan performance under tip-covered inlet condition

The tip-covered screen is one which consists of a mesh covering about 25% of the blade height in the top region.

The comparison of fan performance with tip-covered incident flow is described in Fig. 20. Contrary to performance obtained under hub-covered condition, peak efficiency of three fans is delightfully increased in comparison with that obtained under uniform inlet condition. It is found that the peak efficiency of the fan with 3° forward-skewed angle is increased by 3.02%, the fan with 6° forward-skewed angle by 5.16%, the fan with 12° forward-skewed angle by 0.61%. Moreover, it is observed the stable operating range of three fans is more or less improved. However, as depicted in Fig. 20(a), most part of efficiency curve of the fan with 12° forward-skewed angle is unexpectedly lower than that of the fan with 6° forward-skewed angle, besides the mentioned peak efficiency point. Indeed, this phenomenon can be explained by the following analysis. There should be an optimum forward-skewed angle related to specific aerodynamic demands and geometrical parameters of the fan [22]. And, when the tip-covered screen is mounted and then more amount of mass flow is driven towards blade hub, it is believed that the beneficial effects of forward-skewed blades on the fan performance have been reinforced and more parts of blade loading around tip area have been released. It appears that three fans are being operated as if they were equipped themselves with bigger forward-skewed angle. But, in the case of fan with 12° forward-skewed angle, its ‘immediate’ forward-skewed angle virtually surpasses the optimum angle. At the moment, the incidence angle at leading edge near the blade hub may be increased and the part of the blade can no longer stand too much extra loading so that separation can be found near the hub region on blade pressure side. Therefore, the flow becomes deteriorated and the performance is worsened. All the same, the performance of another two fans is improved to some extends because their 'original' forward-skewed angles are not big enough so that their 'immediate' forward-skewed angles do not exceed the optimum limitation and the performance therefore is being achieved towards the optimum.

The lowest mass flow rate of all three fans is found to become lower and consequently the rotating stall margin will be increased.

Design Point

At design point, the curves of loss coefficients are plotted in Fig.21. As it is anticipated, the overall level of the coefficient is decreased. This beneficial behavior is especially conspicuous near the tip region. In there about 90% span, the coefficient of the fan with 12° forward-skewed angle is decreased by about 1.71% in comparison with that obtained under the uniform inlet condition with the same mass flow rate. But, it is also noted that the fan with 12° forward-skewed angle does not reach the expected performance due to above mentioned reason. Similarly, near the hub region, the coefficient of the fan with 12° forward-skewed angle is not ideal for the same reason. So, it is no doubt that even if a fan is designed with an optimum forward-skewed angle based on assumption of uniform incidence flow, it is impossible for the fan to arrive at the degree of the desired optimum performance if the fan is operated with tip-covered incident flow.

At design point, distributions of tangential velocity of three fans at exit are compared in Fig. 22. Indeed, there is not substantial difference among three curves, except the

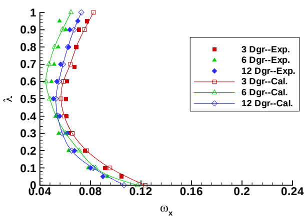

Fig. 21 distribution of loss coefficient along spanwise at design point under tip-covered inlet condition

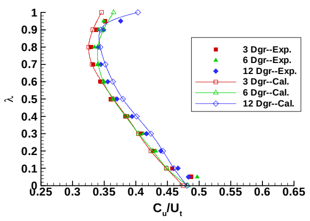

Fig. 22 distribution of tangential velocity coefficient along spanwise at design point under tip -covered inlet condition

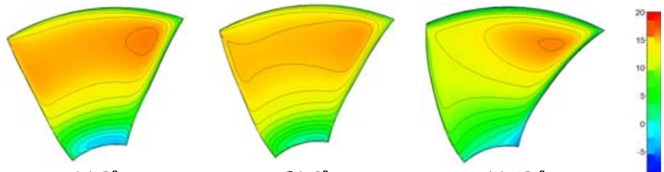

(a) 3° **(b) 6°** **(c) 12 °**

Fig. 23 contours of axial velocity at design point under tip-covered inlet condition

tangential velocity of the fan with 12° forward-skewed angle is a little bigger than those of two other fans. And, contours of axial velocity are depicted in Fig. 23(a), (b) and (c). As shown in these figures, the back-flow regions are suppressed to relatively small size, the contours of axial velocity become much more uniform at exit. Under this inlet condition, not only is the boundary layer accumulation in the tip region controlled so well, but also more kinetic energy is introduced in hub region so that the back-flow region has become smaller and smaller. It is specially shown in the Fig. 23(b) that the corner vortex is almost disappeared, while the vortex can be found in Fig. 23(c). This phenomenon may also be used to explain why under this distorted inlet condition the performance of fan with 6° forward-skewed angle is more excellent than that of the fan with 12° angle at design point as discussed before.

Lower mass flow point

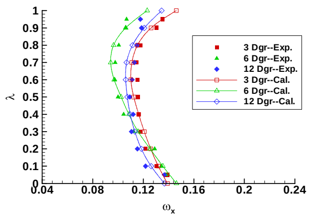

Fig. 24 distribution of loss coefficient along spanwise at lower mass flow point under tip-covered inlet condition

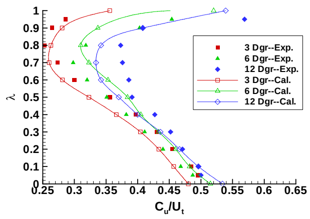

Fig. 25 distribution of tangential velocity coefficient along spanwise at lower mass flow point under tip -covered inlet condition

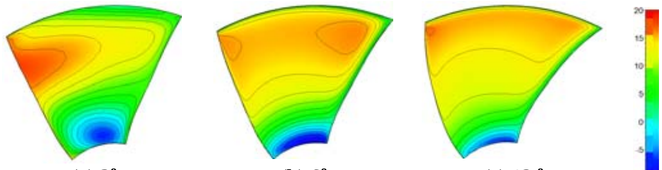

(a) 3° **(b) 6°** **(c) 12 °**

Fig. 26 contours of axial velocity at lower mass flow point under tip-covered inlet condition

Loss coefficient and velocity components of three fans are also compared with each other at the lower mass flow point. It is shown in Fig. 24 that the loss coefficient is still decreased in comparison with that obtained under the uniform inlet condition with the same mass flow rate. The beneficial behavior of the tip-covered screen has still been observed.

And, distributions of tangential velocity and the contours of axial velocity at the point are shown in Fig. 25 and Fig. 26 respectively. In Fig. 25, the tangential velocity of all thee fans is gradually decreased from hub to mid-span, but there is a substantial changing near the tip region where the tangential velocity is swiftly increased. The contours of axial velocity at the point are shown in Fig. 26(a), (b) and (c). And, in these cases, the scale of negative velocity is suppressed to comparatively smaller degree in comparison with that obtained under the uniform condition and the hub-covered condition with the same mass flow rate. It also confirms that all three fans are benefited from tip-covered screen.

Rotating Stall

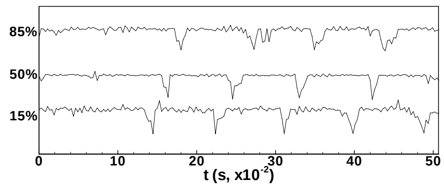

(a)uniform inlet condition

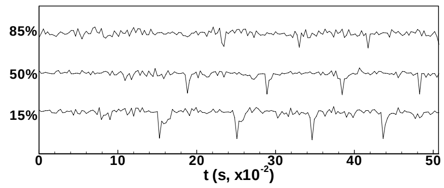

(b) hub-covered inlet condition

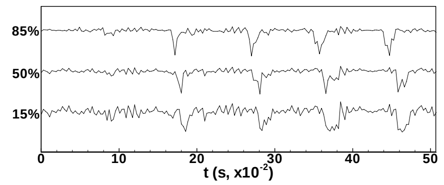

(c) tip-covered inlet condition

Fig. 27 static pressure trace

Fig. 27 shows the static pressure traces in the downstream of the impeller of the fan with 12° forward-skewed angle. The data have been obtained from three radially distributed dynamic pressure sensors under three inlet conditions. The pressure perturbations have been scaled by their mean standard deviations. Granted, the flow in the turbo-machine with lower rotation speed is quite different from that with higher rotation speed in which the flow presents vigorously unsteady characteristic so that the unsteady research is necessary method to study flowing mechanism. But, it is believed that the unsteady research on rotating stall is also helpful to understand the process of stall cells formation in low speed fans with relatively low rotating speed and observe immediate effect of radially distorted inlet condition on fans' rotating stall, especially for the fans with skewed blades.

Under the uniform inlet condition, as shown in Fig. 27(a), stall cells are likely to emerge firstly in the area close to blade hub and then are propagated to rest parts of the blade. It is because there is region near hub where the axial velocity is negative as described in some above mentioned figures. Therefore, the flow separation initially occurs near hub region. When mass flow rate is decreased, this region usually becomes bigger and bigger, separation becomes more deteriorated and flow condition becomes more unfavorable. Then, in the region, it is apt to give rise to formation of the stall cells. Once are the stall cells formed, the original equilibrium along entire span is destroyed immediately and instability is spread from hub to tip consequently.

But, if the hub-covered screen is mounted, as mentioned before, the corner vortex is usually enlarged to bigger area. So, stall cells can be observed at the point with relatively big mass flow rate. It is also noticed from Fig. 27(b) that the stall cells are still formed near hub region and propagated to the rest parts of the blade. But, the transferring rate of stall cells from hub to tip appears to be slowed down somewhat. In this case, more mass flow is collected in the mid-span region and then more kinetic energy is injected into this region. So, the resistance to propagation of instability from blade hub to tip is intensified and transferring rate is decreased.

The result obtained with tip-covered incident flow is shown Fig. 27(c). Stall cells along entire span are almost simultaneously detected under this inlet condition. Indeed, in this case, due to beneficial behavior of tip-covered screen as described before, rotating stall point is delayed to the lowest level. So, when the fan is forced to run near the rotating stall point, the mass flow along entire span is bound to be lower than that under two other inlet conditions, especially in the tip region and mid-span region (Hub region is always occupied by corner vortex.). So, it is believed that incidence angle at leading edge of blade near the tip and mid-span region becomes bigger correspondingly. When mass flow rate is lower than the rotating stall point, stall cells are firstly observed near tip region due to big incidence angle in this area. And because of the relatively low mass flow rate as well as big incidence angle, instability is swiftly propagated to mid-span and then to blade hub.

Similar phenomenon about rotating stall have also been observed when two other fans are mounted and operated under these three different inlet conditions.

CONCLUSION

The aim of this paper is to evaluate the effects of radially distorted incident flow on the performance of fans with forward-skewed blades based on experiments and numerical simulations. For this purpose, the special experimental rig has been set up, including three kinds of screen, such as the uniform screen, the tip-covered screen and the hub-covered screen. And, fans have been respectively manufactured with different forward-skewed angle, 3°, 6° and 12°. In respect of numerical simulation, the k-ω turbulence model is selected to close RANS equations in the paper. The inlet boundary conditions, such as flow rate profile, total pressure, are adopted strictly in accordance with experimental conditions.

Under the uniform inlet condition, the fan with 12° forward-skewed angle has manifested the most excellent performance. The beneficial effect of forward-skewed blades on fan performance is also proved by analysis of loss coefficient profiles along entire span, exit tangential velocity distribution and the contours of axial velocity at both the design point and the lower mass flow point. It is believed that the forward-skewed blades can control mass movement from hub to tip and make blade loading along entire span more uniform. When hub-covered screen is mounted and then an amount of mass flow is compelled to flow through upper part of flow passage, the effects of forward-skewed blades on the fan performance are counteracted and all three peak efficiency is reduced. Even at design point, the larger corner vortex near blade hub can be found. And the situation becomes more deteriorated when fans are operated at the lower mass flow point. By contrast, the effects are reinforced when mass flow is forced to flow towards the blade hub by the tip-covered screen, and the performance of the fans is effectively improved. All three fans are being operated as if they were equipped themselves with bigger forward-skewed angle. Based on these results, it can be reasonably concluded that the performance of fans with forward-skewed blades is literally sensitive to the radially distorted incident flow. Therefore, during the process of aerodynamic design of axial fan, the non-uniform inlet condition must be taken into account.

The data obtained from dynamic pressure sensors reveals that when fans are operated under different radially distorted inlet conditions, pressure fluctuations with time have different modes as the fans are sliding down into rotating stall. With the uniform and the hub-covered incident flow, stall cells usually emerge firstly in the hub region and then instability is propagated to rest parts of the flow passage. All the same, the cells can be firstly found around blade tip region when the fan is operated with the tip-covered incident flow, and then instability is swiftly transferred to mid-span and to hub.

ACKNOWLEDGMENTS

This research was supported by National Nature Foundation (Grants no. 50676054) and National High Technology Research and Development of China (863 Program) (Grants no. 2007AA05Z205).

And the authors wish to acknowledge the financial support from SFC Ventilatoren GmbH & Co. KG.. The authors also gratefully thank to Dr. Martin Renner, for support, assistance and valuable discussions during the development of the project.

REFERENCES

[1] D. P. Harry III and R. J. Lubick, Inlet-air distortion effects on stall, surge, and acceleration margin of a turbojet engine equipped with variable compressor inlet guide vanes, NACA RM E54K26, 1955

[2] D. M. Sandercock and N. L. Sanger, Some observation of the effected of radial distortion on performance of a transonic rotating blade row, NASA TN D-7842, 1974

[3] Z. S. Spakovszky, H. J. Weigl, J. D. Paduano, C. M. van Schalkwyk, K. L. Suder, M. M. Bright, Rotating stall control in a high-speed stage with inlet distortion: Part I-radial distortion, *Journal of Turbomachinery*, Vol. 121 July 1999, pp 510-516

[4] D. C. Leinhos, N. R. Schmid and L. Fottner, The influence of transient inlet distortion on he instability inception of a low-pressure compressor in a turbofan engine, *Journal of Turbomachinery*, Vol. 123 No. 1 2001, pp. 1-8

[5] R. V. Chima, A three-dimensional unsteady CFD model of compressor stability, NASA TM-2006-214117, 2006

[6] C. Hah, D. C. Rabe, T. J. Sullivan and A. R. Wadia, Effect of inlet distortion on the flow field in a transonic compressor rotor, *Journal of Turbomachinery*, Vol. 120 No. 4 1998, pp. 233-246

[7] C. A. Salta and D. G. Kroger, Effect of inlet flow distortion on fan performance in forced draught air-cooled heat exchangers, *Heat Recovery Systems & CHP*, Vol. 15 No. 6, 1995, pp. 555-561

[8] Ch. Jang, S. Choi and K. Kim, Effects of inflow distortion due to hub cap’s shape on the performance of axial flow fan, *Journal of Fluid Science and Technology*, Vol. 3 No. 5 2008, pp. 598-609

[9] Smith, L. H., Yeh, H., Swept and dihedral effects in axial-flow turbomachinery. *Journal of Basic Eng.*, Vol. 85 No. 2 1963, pp. 401-416

[10] S. J. Gallimore, J. J. Bolger, N. A. Cumpsty, M. J.Taylor, P. I. Wright and J. M. M Place, The use of sweep and dihedral in multistage axial flow compressor blading- parts I and II. *Journal of Turbomachinery*, Vol. 124 2002, pp. 521-531

[11] T. H. Carolus, M.G. Beiler, Skewed blade in low pressure fans: a survey of noise reduction mechanism. AIAA-97-1591-CP, 1997

[12] M. G. Beiler, T. H. Carolus, Computational and measurement of the flow in axial flow fans with skewed blades, *Journal of Turbomachinery*, Vol. 108 1986, pp. 32-40

[13] F. A. E. Breugelmans, Y. Carels, and M. Demuth, Influence of dihedral on the secondary flow in a two dimensional compressor cascade, *Journal of Engineering for Gas Turbines and Power*, Vol. 106 No. 3 1984, pp. 578-584

[14] T. Sasaki, F. A. E. Breugelmans, Comparison of sweep and dihedral effects on compressor cascade performance, ASME Paper 97-GT-2, 1997

[15] Test Methods of Aerodynamic Performance for Fans, Standards Press of China, Beijing, China, 2000

[16] D. C. Wilcox, Comparison of two-equation turbulence models for boundary layers with pressure gradient, *AIAA Journal*, Vol. 23 1993, pp. 1414-1421

[17] Menter F.R., Performance of Popular Turbulence Models for Attached and Separated Adverse Pressure Gradient Flows, AIAA Journal, Vol.30 No.8, August 1992

[18] B. Yang, A new blade design scheme for reversible axial flow fan & research on the combined cascades, Dissertation, Shanghai Jiaotong University, 2001

[19] NUMECA Int., 2000, Numeca's Flow Integrated Environment for Turbomachinery and Internal Flows, User Manual, Numeca Int., Brussels, Belgium
[20] Yamaguchi, N., Tominaga, T. and Masutani, Performance improvement by forward-skewed blading of axial-fan moving blades, ISABE 93-7055, 1993, pp580-589
[21] M.Govardhan, O.G.Krishna Kumar, N.Sittaram, Investigation on low speed axial compressor with forward and backward sweep, Journal of Thermal Science, Vol.16, No. 2, 2007, pp 121-123
[22] C. G. Gu and B. Yang, Optimum design of axial flow fan, Technical Report, Key Lab. for Power Machinery & Engineering of Ministry of Education Shanghai Jiaotong University, 2008

APPENDIX: Forward-skewed Angle Equations

It is found in Fig. 1 that on the stacking line the forward-skewed angle θ of a random point with radius r can be obtained by

$$\theta(r) = \theta_{O'} - \angle COO' \quad \text{(A1)}$$

And

$$\angle COO' = \arccos\left(\frac{(r^2 + r_{O'}^2 - R_M^2)}{2rr_{O'}}\right) \quad \text{(A2)}$$

Then, Eq. (A1) can rewritten as

$$\theta(r) = \theta_{O'} - \arccos\left(\frac{(r^2 + r_{O'}^2 - R_M^2)}{2rr_{O'}}\right) \quad \text{(A3)}$$

where, $r_{O'}$ and $\theta_{O'}$ can be determined by the following equations based on $\Delta OHO'$.

$$r_{O'} = \sqrt{r_h^2 + R_M^2} \quad \text{(A4)}$$

$$\theta_{O'} = \arctan(R_M / r_h) \quad \text{(A5)}$$

where, R_M is radius of the stacking line, which can be derived from following equations. It is found from ΔTHO that $\overline{TH}$ can be obtained as following.

$$\left(\overline{TH}\right)^2 = r_t^2 + r_h^2 - 2r_t r_h \cos\theta_t \quad \text{(A6)}$$

where, r_h and r_t are radius of the hub and the shroud respectively, θ_t is skewed forward angle at the blade tip. Also, it is found from ΔTHO

$$\frac{\sin\theta_t}{\overline{TH}} = \frac{\sin(\angle THO)}{r_t} \quad \text{(A7)}$$

Because $\overline{OH}$ is perpendicular to $\overline{O'H}$, $\angle THO$ is

$$\angle THO = \angle THO' + 90° \quad \text{(A8)}$$

Then, Eq. (A7) can be rewritten as

$$\frac{\sin\theta_t}{\overline{TH}} = \frac{\cos(\angle THO')}{r_t} \quad \text{(A9)}$$

And, as the stacking line, $\widehat{TCH}$, is a circular arc, Eq. (A10) can be derived.

$$\cos(\angle THO') = \frac{\overline{TH}}{2R_M} \quad \text{(A10)}$$

Combining Eqs. (A6)-(A10), the radius of the stacking line, R_M, is found to be

$$R_M = \frac{r_t}{2\sin\theta_t}\left(\sin^2\theta_t + \left(\cos\theta_t - \frac{r_h}{r_t}\right)^2\right) \quad \text{(A11)}$$

